Supplementary Information for

Intermittent Proton Bursts of Single Lactic Acid Bacteria

Jia Gao[1], Kai Zhou[1], Haoran Li[1], Yaohua Li[1], Kairong Yang[1], Wei Wang[1]*

[1] State Key Laboratory of Analytical Chemistry for Life Science, School of Chemistry and Chemical Engineering, ChemBIC (Chemistry and Biomedicine Innovation Center), Nanjing University, Nanjing, Jiangsu 210023

Correspondence to: Wei Wang, email: wei.wang@nju.edu.cn.

Table of content

1. Materials and Methods

1.1 Chemicals and Reagents

NaCl, KCl, $MgSO_4$, $MnSO_4$, NaOH, HCl and glucose were obtained from Nanjing Chemical Reagent CO., Ltd (Nanjing,China). 8-Hydroxypyrene-1,3,6-trisulfonic acid, trisodium salt (HPTS), Tetramethylrhodamine methyl ester (TMRM) and RatioWorks™ PH165, NHS easter were purchased from AAT Bioquest. Carbonyl cyanide m-chlorophenyl hydrazine (CCCP) and nigericin were obtained from Shanghai Yuanye Bio-Technology Co., Ltd (Shanghai,China). Sodium monensin was purchased from Proteintech Group, Inc (Wuhan,China). N, N'-dicyclohexylcarbodiimide (DCCD) was purchased from Shanghai Macklin Biochemical Co., Ltd (Shanghai,China). Oligomycin was purchased from Aladdin Holdings Group Co., Ltd (Shanghai,China).

1.2 Strains and culture conditions

The wild-type *Lactobacillus plantarum* (ATCC8014), *Lactobacillus plantarum* (ACCC11095), and *Lactobacillus plantarum* subsp. plantarum were purchased from the BeNa Culture Collection (Beijing, China). The three strains were both grown in MRS broth (Shanghai Dibo Biotechnology Co., Ltd.) at pH 6.9 ± 0.2 at 37°C and incubated at rest.

1.3 Microwell chip device fabrication

Our microwell array chips were fabricated based on the polydimethylsiloxane (PDMS) soft lithography technique.[1] We used CAD software to design the drawing of the microwell array chips, which was processed by Kehua Photomask Co., Ltd. (Jiangsu, China) to obtain the photomask. Using the photomask, master template molds were microfabricated onto 4-inch silicon wafers via a single-step, alignment-free, standard SU8 photolithography process. PDMS chip layers (~2 mm thick) were replicated from the master template molds using 10/1 (w/w) Sylgard184 (Dow Corning). To obtain stable microwell array devices, we used a gasket glass and a cover glass (43 mm × 50 mm, 1000 μm-thick, Fisher, Catalog No. 12-544-1) to fix the PDMS chip layer by oxygen plasma treatment. Procedures for fabricating microwell array devices are provided with more details in **Figure S1**.

1.4 Bacteria loading and digitization

Prior to all experiments, the microwell array devices were placed in a vacuum chamber for >30 min. Buffer-free medium (see Table S1 for medium composition) containing HPTS (AAT Bioquest) and *L. plantarum* cells at pre-determined concentrations were prepared before each experiment. The cover glass of the microwell array device was removed and the prepared sample was immediately loaded into microwells via vacuum-assisted sample loading.[2] Subsequently, a layer of paraffin oil (~100 μm) was used to seal the microwells and prevent evaporation of the droplets. Detailed experimental procedures for preparing, loading, digitizing and detecting bacteria in microwell array devices are explained extensively in **Figure S1** & **S3**.

1.5 FL-pH titration of HPTS

A 30 ml beaker was filled with 20 ml of simple culture medium and 2 mM of the pH-sensitive dye HPTS. The pH was adjusted by adding NaOH (0.2 M) or hydrochloric acid (1 M) dropwise with stirring. A Sartorius PB-10 pH meter was carefully calibrated and used to measure the pH of this solution. At a fixed pH, 1 ml of this solution was taken as a sample. In accordance with the experimental conditions, the FL intensity of the solution was measured at different pH values under fixed excitation and emission conditions, and the relationship between pH and FL intensity was finally obtained (**Figure 2d**).

1.6 Introduction of TMRM and RatioWorks™ PH165, NHS ester to cells

A commercially available membrane potential-sensitive fluorescent dye, TMRM, was used to report bacterial membrane potential in real time. *L. plantarum* cells were incubated with 10 μM TMRM in PBS solution (containing 2% glucose) for 1 hour. These bacteria were then centrifuged and washed with PBS solution (containing 2% glucose) at 6500 rpm for 2 min and repeated three times until the unbound dye was completely removed (the supernatant became colorless).

RatioWorks™ PH165, NHS ester is a fluorescent dye that is suitable for ratiometric determination on intracellular pH. Bacteria were incubated with 10 μM PH165, NHS ester, in PBS solution (containing 2% glucose) for 45 minutes. Then bacteria were centrifuged and washed with PBS solution (containing 2% glucose) three times prior to immobilization.

1.7 Microscope apparatus

The experiments were performed on a commercial inverted FL microscope (Nikon, Ti-E), which was equipped with a 20× objective lens with a numerical aperture (N.A.) of 0.40. A white-light source (X-cite 110 LED, Excelitas Tech.) coupled with a band-pass filter (488/18 nm, Semrock) was used to excite the FL of pH sensitive dye HPTS. A sensitive digital CMOS camera (C11440, Hamamastu) was used to collect the FL signals of HPTS. Typical exposure settings were 500 ms (2 fps). A dichroic mirror (505 nm, Semrock) and a band-pass filter (505-555 nm, Semrock) were placed in the microscope filter cube to discard the excitation light.

The microscope filter cube was adjustable for different FL imaging. For TMRM measurements, FL of TMRM was excited at 561 nm (561/14nm filter, Semrock) and collected at > 594 nm (594 nm long-pass filter, Semrock), where a dichroic mirror (590 nm long-pass, Semrock) was used to separate the excitation and emission light. For RatioWorks™PH165 NHS ester measurements, the same 561 nm excitation filter, 590 nm long-pass dichroic mirror but another emission filter (650 nm long-pass, Semrock) were combined to acquire FL images.

Simultaneous recording of dual FL (pH_e and Ψ_m, pH_e and pH_i) were acquired using a 60× oil immersion objective (N.A.=1.49, Nikon). A self-written MATLAB code was used to control the automatic switching of the microscope filter cubes with the corresponding filter set for each

type of FL signals. The acquisition rate was one image every 5 seconds (0.2 fps). All FL images were analyzed using ImageJ software and custom MATLAB code.

2. Supporting Figures

2.1 Preparation of microwell array chip and generation of microdroplets

In a typical procedure for chip preparation, PDMS polymer base and curing agent (Sylgard184, DowCorning) were first mixed in the ratio of 10/1 (w/w) and degassed for 0.5 h under vacuum. Next, this mixture was gently poured onto the master template (with micropillar arrays of 10 μm diameter and 20 μm height) and cured at 65 °C for 1 h. After cooling to room temperature, the PDMS was then peeled off from the silicon master mold and cut into small pieces with desired sizes. The thickness of the fabricated PDMS chip was approximately 2 mm, and the PDMS chips can be used immediately or stored in a clean plastic vial for later use (**Figure S1a**). In order to obtain stable microwell array chip devices, we used a gasket glass and a cover glass (Fisher, Catalog No. 12-544-1, 1000 μm-thick) to fix the PDMS chip with the help of oxygen plasma treatment. Specifically, the patterned side of the PDMS chip layer with microwells was first bonded to the cover glass to prevent its exposure to oxygen plasma. Then the other flat side of the PDMS chip and the gasket glass were treated with oxygen plasma for 3 min and brought into contact immediately. A sandwich structure was formed and baked at 60 °C for 5min. All PDMS microarray chip devices were stored at 60°C for at least 12 hours prior to use to ensure their hydrophobicity (**Figure S1b**).

In this work, the bacteria can be efficiently loaded into the microwell arrays by vacuum-assisted sample loading and oil-driven encapsulation. The plasticity of the PDMS material determined that the evacuation operation can create a negative pressure within the chip devices and caused the deformation of microwells to reach a vacuum state. The coverslip was then removed and the prepared bacterial sample was immediately added within 10 seconds. The liquid sample can be successfully fulfilled in the microwells during shape recovering of PDMS. Paraffin oil was then added onto the empty surface of the PDMS chip, and a coverslip was used to gently slide the oil droplets along the chip surface to the sample-covered area. Due to the hydrophobic nature of PDMS, the sample solution on the hydrophobic surface was replaced by a layer of oil and the droplets were effectively encapsulated in the microwells. The oil layer also sealed the droplets to prevent evaporation (**Figure S1c**).

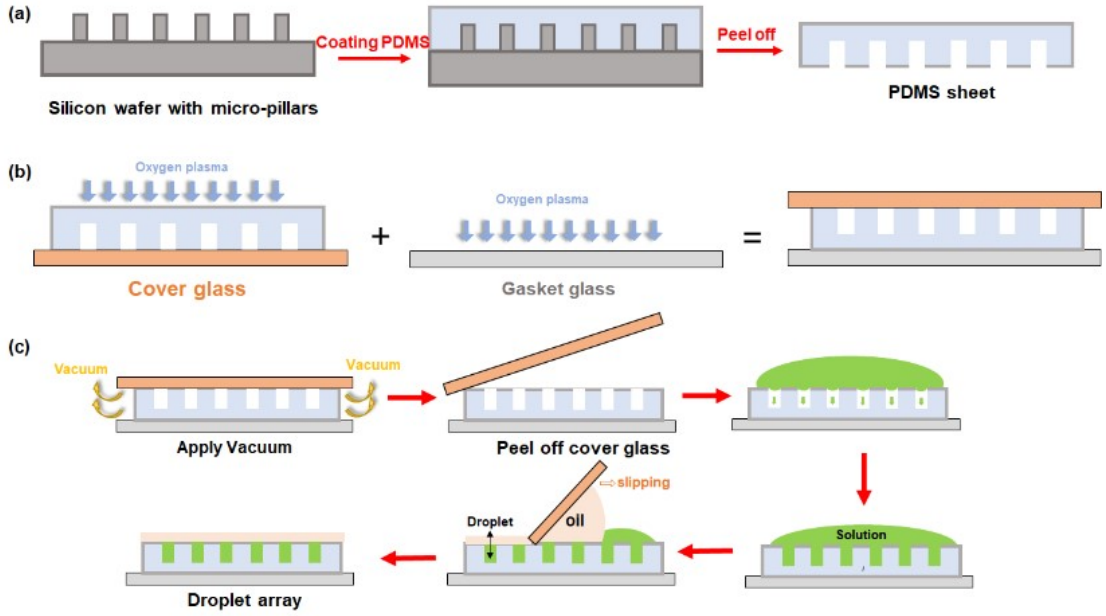

Figure S1. Flow chart for (a) the fabrication of PDMS chip, (b) PDMS microwell array chip device preparation and (c) the oil-covered droplet array preparation procedure.

2.2 Threshold method for differentiation of occupied (active) and unoccupied microwells

Figure S2a shows a representative FL image of about 600 microwells in the observation area after incubation for about 20 minutes. We extracted the FL kinetics curve of each microwell, calculated the FL decay rate of each microwell in the first 100 seconds, and plotted the FL decay rate in the histogram (**Figure S2b**). The histogram shows a smaller subpopulation of weakly fluorescent microwells that containing *L. plantarum* (*i.e.*, active wells) and a larger subpopulation of strongly fluorescent empty microwells (*i.e.*, unoccupied wells), with a ~ 5-fold difference in the FL signals between the two populations (**Figure S2c** & **Figure S2d**).

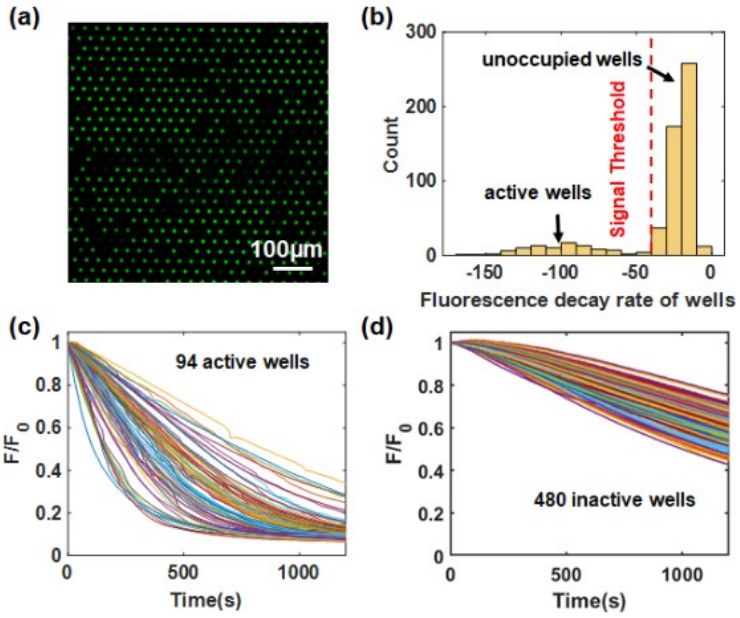

Figure S2. (a) FL image of the microdroplet array, where the microwells with active bacteria showed weaker FL intensity. (b) Histogram of FL decay rate for all microwells during the first

100 s. The histogram showed a weakly fluorescent subpopulation of microwells with the presence of bacteria (active wells) and a strongly fluorescent subpopulation of empty microwells without bacteria (unoccupied wells), and the signal threshold (red dashed line) was added to separate the two subpopulations. (c, d) Kinetics of FL intensity changes in the separated active and unoccupied wells using signal threshold.

2.3 The random encapsulation of individual bacteria following the Poisson's distribution law

The concentration of bacterial samples was measured by flat colony counting method. Briefly, *L. plantarum* cells were collected at the logarithmic growth stage and washed three times with fresh MRS culture medium. This bacterial suspension was then diluted 4, 6, 8, and 10 times with fresh culture medium and the OD values at 600 nm were determined for the corresponding concentrations using a multifunctional microplate reader (Biotek Synergy H1). The four diluted samples were further diluted 10^5, 10^6, 10^7 times to obtain 12 samples, then 200 µl of each of the 12 samples were plated on solid plates. All plates were incubated at 37°C for 24 h. After incubation, the number of colonies on each plate was manually counted. The number of counted colonies was plotted against the OD_{600} value and a linear fit was performed. Finally, if necessary, the bacterial sample concentration can be recalculated using the slope of the linear fit line and the OD value of the bacterial solution (**Figure S3a**).

Stochastic confinement of single bacteria in microwells is a Poisson process. The probability of finding x bacteria in a microwell is given by **eqn (1)**, where λ is the average number of bacteria per microwell, as determined by product of the concentration of bacteria in solution and the microwell volume. To validate the reliability of the method, we loaded 1.2×10^8 CFU/mL of pre-quantified *L. plantarum* cell suspension onto our microchip arrays. According to the Poisson distribution law, this concentration would result in an average occupancy (λ) of approximately 0.2 in our microwell array (1.57 pL-sized microwell), *i.e.*, approximately 20% of the picolitre microwells were expected to be occupied by individual bacterial cells. Using this method, we observed approximately 15.7% randomly distributed weakly fluorescent microwells within the imaging region, which is in line with our expectations and strongly supported the random distribution of individual bacteria according to the Poisson distribution (**Figure S3b**& **Figure S3c**).

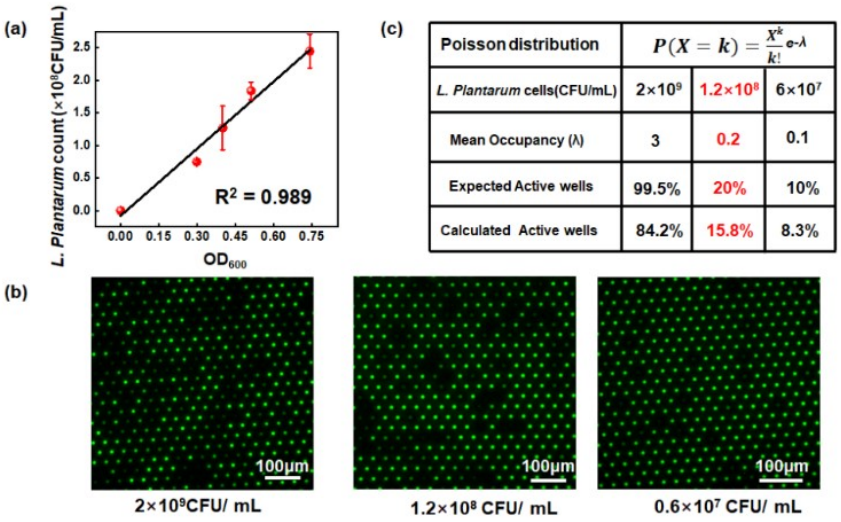

(c)

Poisson distribution	$P(X=k)=\frac{X^k}{k!}e^{-\lambda}$		
L. Plantarum cells(CFU/mL)	2×10^9	1.2×10^8	6×10^7
Mean Occupancy (λ)	3	0.2	0.1
Expected Active wells	99.5%	20%	10%
Calculated Active wells	84.2%	15.8%	8.3%

Figure S3. (a) Relationship between the number of *L. plantarum* and OD_{600} values. (b) End point FL images of three independent experiments with different concentrations of *L. plantarum* samples. (c) The number of active wells predicted by the Poisson distribution versus the number of active wells counted from experiments.

As a complementary proof, we also performed experimental acquisition at a lower magnification objective to observe more microwells, as shown in **Figure S4**. We statistically analyzed 9 different regions within the field of view containing 6,795 microwells to count the spatial distribution and number of active microwells. The statistical results in Figure R4b showed that the proportion of active microwells in different regions was basically the same. It indicated that the distribution of bacteria was indeed spatially random.

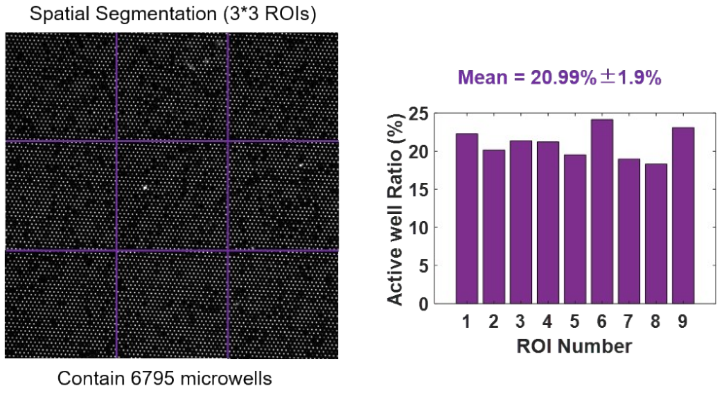

Figure S4. Statistical analysis of more microwells revealed a uniform distribution of bacteria.

2.4 Subtraction of fluorescent background caused by photobleaching

During the reaction, continuous excitation light irradiation inevitably caused photobleaching of both active and unoccupied wells. Due to inhomogeneity of the illumination, we selected the unoccupied wells (blue circles) around the active well (red circle) as the photobleaching background and subtracted them.

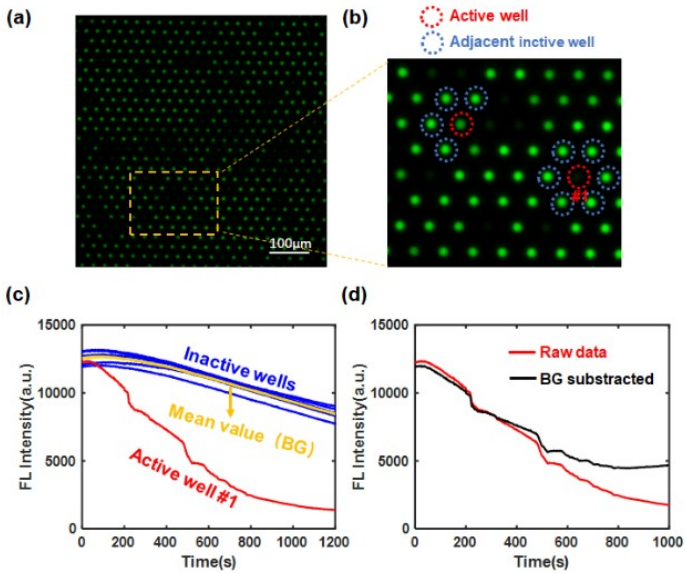

Figure S5. (a) FL image of the microwell array. (b) Zoom-in FL images of several microdroplets from (a), where red circles indicated active microwells and blue circles indicated unoccupied microwells in adjacent regions. (c) FL change kinetics of active well #1 and adjacent unoccupied wells. The yellow curve is the average of kinetic curves of six unoccupied microwells as a background to the FL of active well #1. (d) Original FL curve of active well #1 and the FL curve after subtraction of the background.

2.5 Similar proton burst phenomenon observed in microdroplets generated by the mechanically sealed method

Mechanical pressure sealing is another commonly used method for droplet sealing.[3, 4] We used this method to investigate the effect of oxygen content on the proton release behavior of *L. plantarum*. In this experiment, we used PDMS microwell array chips with a thickness of 2 cm and 1 mm-thick-glass coverslips to effectively prevent oxygen diffusion as well as microwell deformation caused by mechanical pressure. The entire chip was then placed in a sealed chamber (formed by an array holder) to further prevent oxygen ingress (**Figure S6a**). The bacterial sample preparation method and the droplet loading method were kept consistent with the context. Using this method, the same proton burst event was observed, and the time scale and kinetic characteristics of the burst events were consistent with those obtained in the oil-sealed method (**Figure S6b**). It indicates that the proton burst release phenomenon exists under both aerobic and anaerobic conditions.

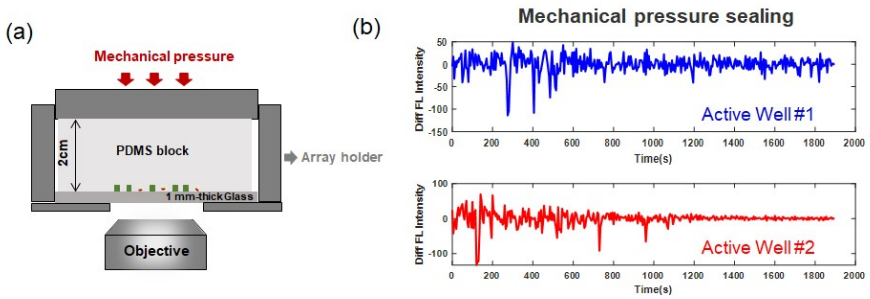

Figure S6. The same proton burst event was observed when using a mechanical pressure sealing method to create an oxygen-free environment.

2.6 Automated detection of proton burst events

The automatic detection of proton burst events was realized using a threshold-based algorithm and self-developed MATLAB code based on our previous approach.[5,6,7] The overall detection scheme was divided into three main steps: 1. image pre-processing to reduce noise and image drift, 2. extraction of microwells, and 3. event detection and parameter extraction.

Image pre-processing. A dark image was first subtracted from the experimentally captured image sequences to eliminate the dark current background of CMOS camera. Next, we conducted image denoising by averaging every 10 frames, resulting image acquisition rate from 2 frames per second (fps) to 0.2 fps. To remove image drift, we utilized a previously proposed image pixel reconstruction algorithm.[7]

Microwell extraction. The reference fluorescence image at the start stage without acidification was obtained by averaging the first 5 frames of the image sequence (**Figure S7a**). To extract the edges and locations of the microwell automatically, we first use image binarization function to change the reference image to a binary picture with a threshold of 20% maximum value of raw image. Then "bwlabel" function in MATLAB was used to obtain the region of interest (ROI) for each microwell (**Figure S7b**). Subsequently, the time trajectory curve was obtained by calculating the average fluorescence intensity of each ROI at every time point (**Figure S7c**).

The initial fluorescence decline rate of the kinetic curve (**Figure S2b**) was used to distinguish the microwells with bacteria from the blank microwells. To remove potential photobleaching effects, we subtracted the fluorescence of the empty wells beside the active wells as a photobleaching background (see **Figure S5**).

Event detection and parameter extraction. The obtained active microwells' kinetic curves were normalized by dividing them by the value at t = 0 (**Figure S7d**). To obtain the proton bursts' spike events, the fluorescence kinetic curves were differentiated (see **Figure S7e**). By using Fourier transform, any noise signals at low and high frequencies were removed and the curve's baseline was flattened to near 0 (see **Figure S7f**). Burst events differ from non-burst events based on the spike intensity magnitude. Typically, we established a threshold in this study to differentiate these two states. If the change in fluorescence intensity exceeded the threshold of -0.3% (which was determined by calculating approximately six times the standard deviation of the baseline, 6*STD, in this analysis), it will be regarded as a proton burst event. On the contrary, if the fluorescence intensity fluctuated below this threshold, it will be considered a non-proton burst state (refer to **Figure S7g**). The number of events was determined by extracting the number of the peak, and the width of the peak was defined as the time duration for the burst event.

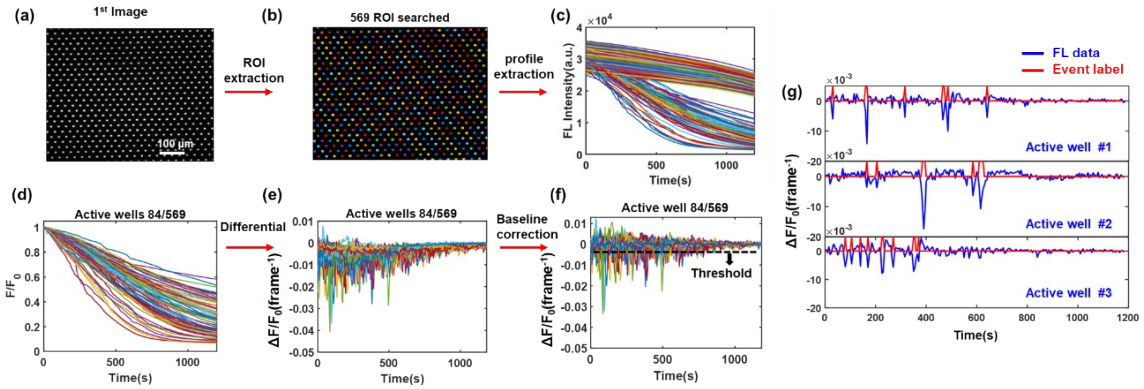

Figure S7. (a)-(g) The overall detection scheme of proton burst events. Image frame rate, 0.2 fps.

Determination of $k_{constant}$ and k_{burst}. The "findpeaks" function in MATLAB was utilized to identify the peaks' location, t_n. The values in the time range from (t_n -50s) to (t_n +50s) were extracted from the original fluorescence curves to determine the kinetics of an individual proton outburst (**Figure S8a** & **Figure S8b**). A linear fit of five time points (2.5s) ranging from (t_n -1s) to (t_n +1s) yielded the slope as the rate constant for the burst event, k_{burst}. A linear fit of the initial 20 data points (10 seconds) in each event yielded the fundamental decay rate, $k_{constant}$ (**Figure S8c**).

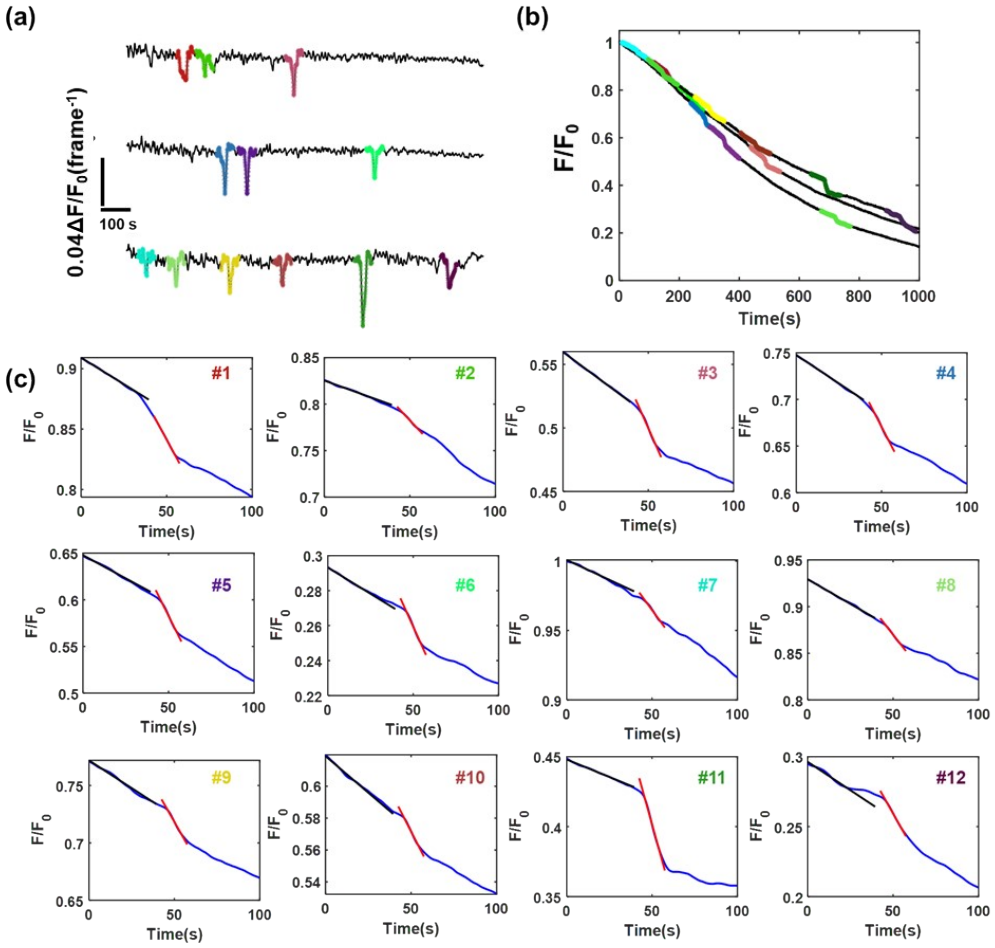

Figure S8. The determination of $k_{constant}$ and k_{burst}. Image frame rate, 2 fps.

2.7 A representative intense proton burst event

Figure S9 shows a strong proton burst event with a K_{burst} to $K_{constant}$ ratio of 8.3, indicating an intense proton efflux during the burst events.

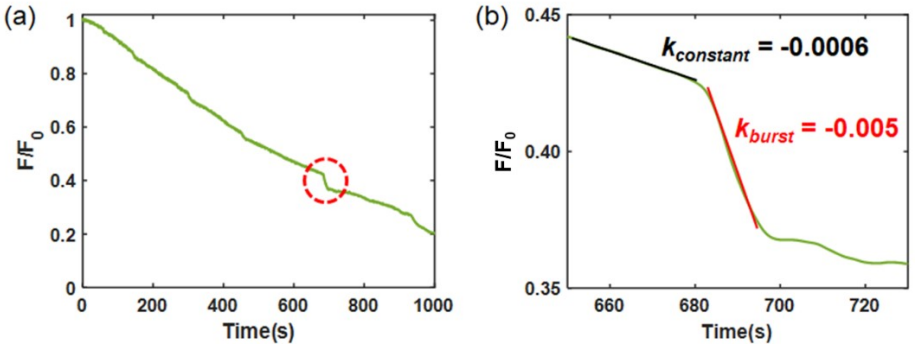

Figure S9. A representative intense proton burst event.

2.8 Influence of DCCD and oligomycin on the average proton release rate of bacteria

Averaging all the kinetic curves in **Figure 3d** and **Figure 3e** yielded the average kinetic curves (**Figure S10a** and **Figure S10b**), which represent the acid-producing activity of bacteria at the ensemble level. As shown in **Figure S10**, although the proton burst event was inhibited in the presence of DCCD and oligomycin, the constant proton release process was still present. This result supports that the constant proton release process represents the passage of intracellular protons across the cell membrane in the form of lactate-neutral molecules.

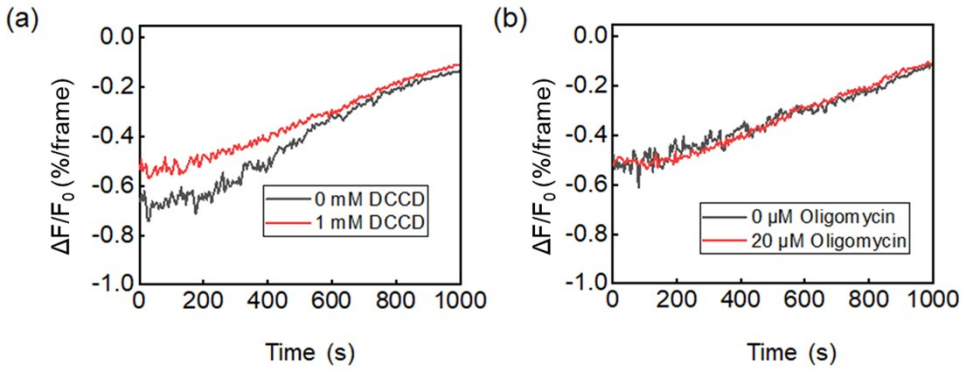

Figure S10. The average proton release rate of bacteria with (black curve) and without (red curve) the addition of DCCD (a) and oligomycin (b). It shows that the addition of inhibitor had almost no effect on the proton release rate of bacteria. Image frame rate, 2 fps.

2.9 Proton bursts in other two strains of lactic acid bacteria

Proton bursts were also observed in two other lactic acid bacteria, *L. plantarum*

subsp.plantarum (**a**,**b**) and *L. plantarum* ACCC11095 (**c**,**d**). These results demonstrate the universality of the bacterial proton burst phenomenon.

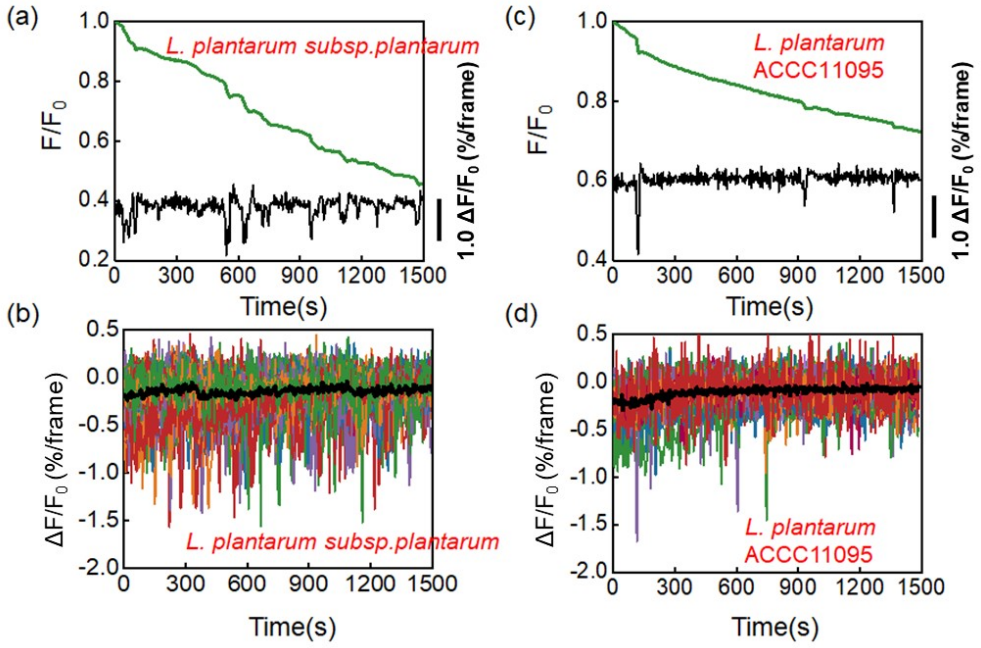

Figure S11. (a) Representative FL curve (green) and the corresponding proton burst trajectory (black) of a single *L. plantarum* subsp.plantarum. (b) Differential FL curves of active microwells showing intensive proton burst events. The black bold curve represents the average results of all the active microwells. (c) Representative FL curve (green) and the corresponding proton burst trajectory (black) of a single *L. plantarum* ACCC 11095. (d) Differential FL curves of active microwells showing sparse proton burst events. The black bold curve represents the average results of all the active microwells. Image frame rate, 2 fps.

2.10 Synchronized proton bursts and membrane potential fluctuations in *L. plantarum*

Figure S12 shows four representative records related to extracellular protons (HPTS, green) and membrane potential (TMRM, red). A simultaneous decrease is observed in both curves, indicating that the burst of protons is accompanied by a simultaneous depolarization of the membrane potential.

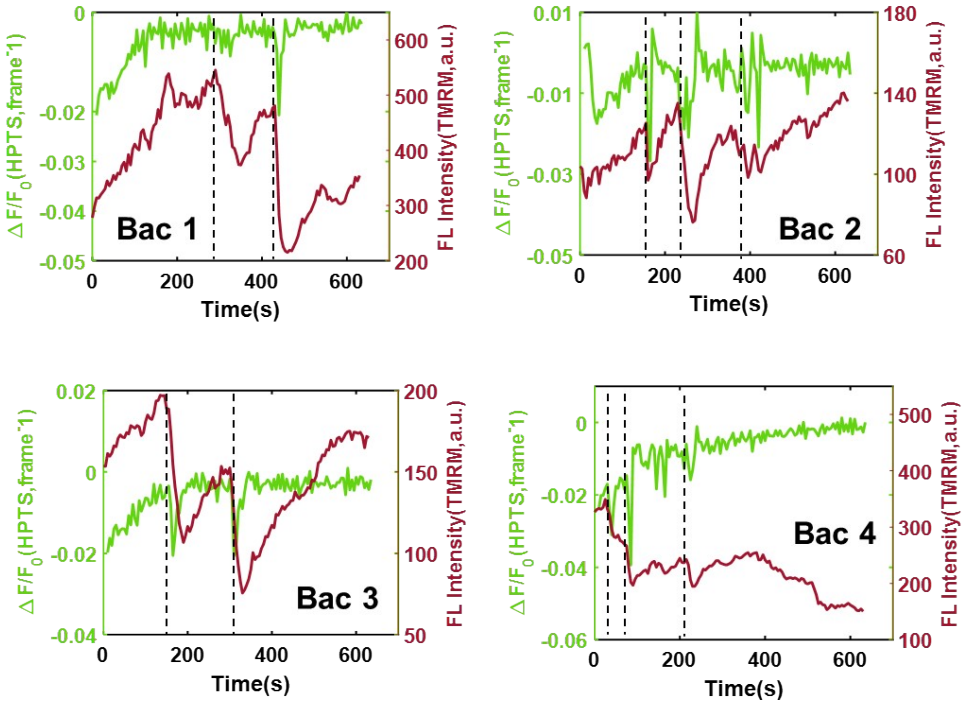

Figure S12. Correlative pH_e (green curves) and Ψ_m (red curves) recordings of four representative *L. plantarum* labeled by TMRM, a membrane potential sensitive dye. Image frame rate, 0.2 fps.

2.11 Measurement of HPTS response time

As illustrated in **Figure S13**, a device for detecting fluorescence was established to calculate the response time of HPTS. A vertical blue excitation light was projected onto the base of a 3 mL beaker to excite the fluorescent dye HPTS. A camera was placed perpendicularly to the excitation light to capture the emitted fluorescence of the dye. A green band-pass filter was positioned in front of the camera to filter out excess light from the surroundings. The experiment was carried out in darkness with careful insulation from scattered ambient light. The dye concentration, solution composition, and pH in the beaker were maintained identical to the conditions in the microwells. With a camera frame rate of 50 per second (20 ms exposure time), 0.1M HCl was added dropwise to the beaker with sufficient magnetic agitation, controlling the solution pH change, and recording the fluorescence intensity change as demonstrated in **Figure S13b**. The HPTS response time during pH decrease is determined to be 100 ms (pH 6.5 to pH 6.0) and 450 ms (pH 6.0 to pH 5.0), respectively. Hence, the HPTS

response time was shorter than the camera recording time of 500 ms in the microwell experiment. This result confirmed the validity of detecting proton burst events using HPTS.

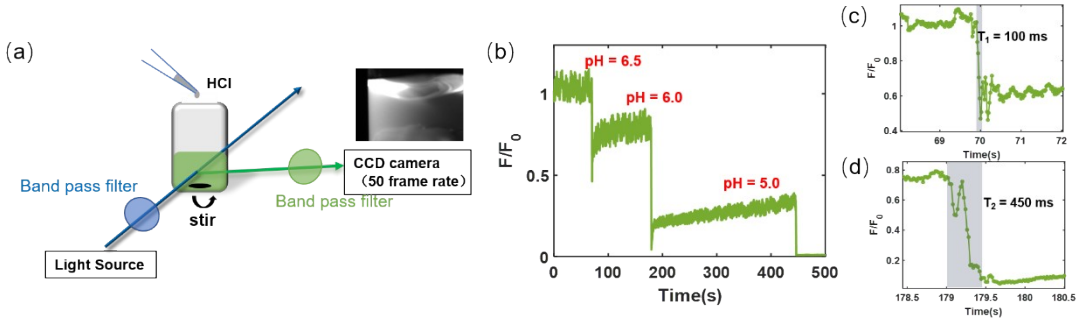

Figure S13. (a) Schematic diagram of fluorescence acquisition device. (b)-(d) Response time of HPTS.

3. Supplementary Tables

3.1 Chemical composition of simple culture medium

The composition of the simple culture medium is based on the normal *L. plantarum* culture medium (MRS culture medium) with the removal of easily adsorbed protein molecules and potential buffering substances. Glucose was used as a carbon source to maintain normal cell metabolism, NaCl and KCl were used to maintain osmotic pressure, and Mg^{2+} and Mn^{2+} are cofactors for enzyme activity. The pH of the culture medium was adjusted with dilute NaOH/HCl. 2 mM HPTS was added to the culture medium when FL experiments were performed. This simple culture medium formulation was suitable for the study of proton-related metabolism in *L. plantarum*.

Chemicals	Concentration (mM)
Glucose	111
NaCl	120
KCl	8
$MgSO_4$	1.67
$MnSO_4$	0.3

Table S1. Chemical composition of simple culture medium.

3.2 Gene and amino acid sequences of H^+-ATPase in *L. plantarum* strains

Gene sequencing of the three strains was performed by Sangon Biotech Co., Ltd. (Shanghai, China) using Illumina HiSeq and PacBio RSII systems. Sequence assembly was performed using SPAdes. Sequence correction was performed using PrInSeS-G. Gene functional annotation was based on CDD, KOG, COG, NR, NT, PFAM, Swissprot and TrEMBL databases. The results showed that *L. plantarum* strains indeed contained the H^+-ATPase gene.

Gene sequences:
ATGGGAGCAATTGCTGCAGGTATTGCTATGTTTGGTGCCGCTTTAGGTGCTGGTA
TTGGTAACGGTTTGGTTATTTCTAAGATGCTTGAAGGGATGGCCCGTCAACCAGA
ATTATCTGGTCAATTACGGACTAACATGTTCATCGGTGTTGGGTTGATCGAATCA
ATGCCTATCATTTCCTTCGTTGTTGCTTTGATGGTTATGAACAAGTAA
Amino acid sequence:
MGAIAAGIAMFGAALGAGIGNGLVISKMLEGMARQPELSGQLRTNMFIGVGLIESMP
IISFVVALMVMNK

Table S2. Gene and amino acid sequences of H^+-ATPase in *L. plantarum* strains.

4. Description of Supplementary Movies

Movie S1. Metabolic acid production kinetics of a single *L. plantarum* bacterium in each occupied microwell.
Movie S2. Proton burst phenomenon of a single *L. plantarum* bacterium in each occupied microwell.

5. References

1. Y. N. Xia and G. M. Whitesides, Soft lithography, *Annu. Rev. Mater. Sci.*, 1998, **28**, 153-184.
2. L. Xu, H. Lee, D. Jetta and K. W. Oh, Vacuum-driven power-free microfluidics utilizing the gas solubility or permeability of polydimethylsiloxane (PDMS), *Lab Chip*, 2015, **15**, 3962-3979.
3. R. B. Liebherr, A. Hutterer, M. J. Mickert, F. C. Vogl, A. Beutner, A. Lechner, H. Hummel and H. H. Gorris, Three-in-one enzyme assay based on single molecule detection in femtoliter arrays, *Anal. Bioanal. Chem.*, 2015, **407**, 7443-7452.
4. J. Gao, H. Su and W. Wang, A microwell array-based approach for studying single nanoparticle catalysis with high turnover frequency, *J. Chem. Phys.*, 2021, **155**, 071101.
5. Yimin Fang, Zhimin Li, Yingyan Jiang, Xian Wang, Hong-Yuan Chen, Nongjian Tao, Wei Wang, Intermittent photocatalytic activity of single CdS nanoparticles. *Proc. Natl. Acad. Sci. USA*, 2017, **114**, 10566-10571.
6. Yaohua Li, Haoran Li, Jia Gao, Ben Niu, Huan Wang, Wei Wang, Visualization of the intermittent gating of Na+/H+ antiporters in single native bioluminescent bacteria, *Angew. Chem. Int. Ed.*, 2023, 62, e202215800.
7. Jia Gao, Xiang Wo, Yongjie Wang, Minghe Li, Chunyuan Zhou, Wei Wang, A post-recording pixel-reconstruction approach for correcting the lateral drifts in surface plasmon resonance microscope, *Anal. Chem.*, 2019, **91**, 13620-13626.